

Model of Total Skin Electron Treatment Using the 'Six-Dual-Field' Technique

Dario Faj¹, Mladen Vrtar¹, Zdenko Krajina¹, Slaven Jurković²
and Damir Margaretić³

¹ University Hospital »Osijek«, Osijek, Croatia

² University Hospital Center »Zagreb«, Zagreb, Croatia

³ University Hospital Center »Rijeka«, Rijeka, Croatia

ABSTRACT

During implementation of the total skin electron treatment, using six-dual-field technique, at radiotherapy department a large number of measurements are needed. To assess depth dose curve required by clinicians and dose uniformity over a whole treatment plane, combinations of different irradiation parameters are used (electron energy, beam angle, scatterers). Measurements for each combination must be performed. One possible way to reduce number of measurements is to model the treatment using the Monte Carlo simulation of electron transport. We made a simplified multiple-source Monte Carlo model of electron beam and tested it by comparing calculations and experimental results. Calculated data differs less than 5 percent from measurements in the treatment plane. During the treatment patient can be approximated using cylinders with different diameters and orientations. We tried to model the depth dose variations in the total skin electron treatment not just around the body cross-section (simplified to cylinders of different diameters), but also along the body to account for the variations in body curvature longitudinally. This effect comes down to the problem of modeling distribution in different cylinders, but varying the longitudinal orientation of those cylinders. We compared Monte Carlo calculations and film measurements of depth dose curves for two orientations of the cylindrical phantom, which were the simplest for experimental arrangement. Comparison of the results proved accuracy of the model and we used it to calculate depth dose curves for a number of other cylinder orientations.

Key words: radiotherapy, mycosis fungoides, skin, electron, model

Introduction

The total skin electron treatment (TSET) appears to be one of the most effective treatments for superficially widespread cutaneous T-cell lymphoma or other malignancies involving multiple sites of skin¹⁻⁵. The TSET is irradiation of the whole skin with the prescribed absorbed dose to a certain depth. At our department we use the 'six-dual-field' technique⁶. The related reference concentrates almost exclusively on idealized conditions, such as the *in-air* distribution of radiation and the dose received by cylindrical phantoms⁶⁻⁹.

Implementation of the technique at the radiotherapy department requires a large number of measurements. To assess required dose uniformity over the treatment plane and satisfying depth dose curve, a combination of different irradiation parameters (electron energy, beam angle, different scatterers) must be measured¹⁰. A way to reduce number of measurements is to use the Monte Carlo (MC) modeling of the beams. We used the multiple source model¹¹. To test the model, the results of the MC calculations are compared with the *in-air* measurements. Comparison with the measurements justified the assumption that lots of electrons scattered from collimator and electron applicator will not reach treatment plane. To simplify the model and to save the computation time we discarded those electrons.

After the TSET, additional doses with local fields are applied to the under dosed areas as determined by *in-vivo* measurements of the absolute dose¹². At the points where the *in-vivo* measurements are performed, the depth dose curves are assumed to be the same as the measured depth dose curve in the cylindrical phantom of 30 cm diameter and height. The phantom is normally oriented to the axis of a beam and irradiated with all the six pairs of beams^{10,12}. That cylinder represents the trunk of an average patient. It

had already been shown that if a diameter of the cylinder was changed, there would also be a change of the depth dose curve⁸. In reality, not only diameters of body cylinders are changing, but they are also angled in respect to the beam axis. Any angle is possible (e.g. forearms) and the axis of rotation is not always the axis of the cylinder (e.g. shoulders). To validate our model and to show possible variations in depth dose curves, we compared depth dose curves in two different, measurable body cylinder orientations. Also, calculations of depth dose curves for a number of different, hard-to-measure orientations of cylinders are done.

Materials and Methods

The Siemens Mevatron MD2 was used to produce 5 MeV electron beams to treat patients with mycosis fungoides. A dose of 30 to 35 Gy is delivered to depths of 5 to 10 mm in nine weeks, four fractions a week. The 'six-dual-field' technique with patients in the standard positions¹⁰ was used. Patients were irradiated in a standing position 3.5-m from the isocenter and 0.5 cm scatterer made of clear Lucite is interposed in the beam to obtain the required depth dose curve (Figure 1).

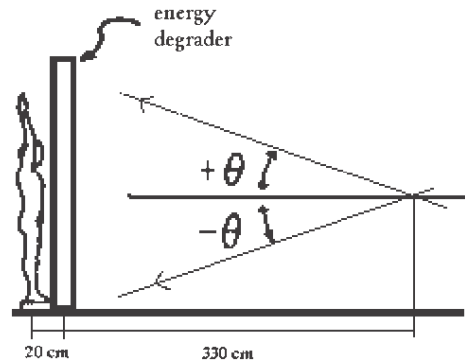


Fig. 1. Two angle beams are combined to cover the patient's height. An energy degrader is put in front of the patient at the 20-cm distance.

Scattering in a layer of 3.5 m of air significantly degraded the electron energy of a beam. In addition to the change of energy, the beam was considerably widened in size and it exhibited the »Gaussian« distribution with an »80% to 80%« width of approximately 80-cm. It was uniform enough to cover the patient's width. In vertical direction it was necessary to combine two beams. The angle \varnothing shown in Figure 1 was found to be 10 degrees. The dose uniformity over the patient's height, achieved by two angled fields, was proved to be satisfactory by film dosimetry.

Depth dose distributions and dose profiles in the treatment plane were measured by the Marcus plan parallel ionization chamber in the PTW solid phantom type 29672. For electron dosimetry, the PTW phantom shows negligible deviations in relative measurements, as has been confirmed¹³. Depth ionization curves obtained with the Marcus chamber are converted to depth dose curves by correcting for changes in stopping power ratios with depth¹⁴. During the measurements the cable was shielded with lead to avoid irradiation-induced ionization.

Relative measurements were also made using XV2 Kodak photographic films, what is useful for investigating the distributions obtained when multiple fields are combined. The cylindrical phantom was made of 2.5-cm slabs of PMMA with 30-cm diameter and height. In the dark room the film was clamped between the central slabs and trimmed with a razor blade to match the circular cross section of the phantom. A film was fixed between two slabs by a screw and a nut. The edge of the film was then covered with a layer of black electrical tape to make a light-tight seal. We must point out that most problems in the film dosimetry appeared due to cutting and aligning film into the phantom. In comparison to other measurements we used the water equivalent radiological thickness for PMMA of 1.115¹⁵ and all measurements were expressed in

cm of water. The film was developed and the optical density was measured using transparency scanner Colorpage HR5 Pro (Genius) and our own program package. After the scanning (which was always performed under precisely same conditions) an 8-bit pixel BMP image was obtained. Our gray scale was given by integers 0-255, the higher number meaning higher exposure. The sensitometric curve (optical density as a function of an absorbed dose) was measured previously.

To test the MC model we also performed measurements at the standard 'source-to-phantom distance' (SPD) of 100 cm. All measurements at the SPD = 100 cm are done in the Wellhöfer blue water phantom using a p-type silicon diode. Because the variation of 'silicon-to-water' stopping power ratio with energy is relatively small (~5% between 1 and 20 MeV) we used data obtained by a diode directly as the depth dose curve.

The Monte Carlo model of the beam

The MC simulation is done with the EGS4 system for simulating radiation transport¹⁶, using a user-written interface based on the DOSRZ code (see <http://www.slac.stanford.edu/egs/>). The DOSRZ code is the EGS4 user code that simulates the passage of an electron or a photon beam in a finite, cylindrical geometry. The user defines the geometry of the target via the input of a number of planar and cylindrical coordinates that divide the cylinder into a number of regions. Also, the user must specify the regions where the dose is to be scored and the type of source of radiation. All the geometrical checks of crossing 'geometrical' or 'dose' regions are handled by the subroutine HOWFAR of the DOSRZ code. Since the used geometry is finite, we used the half value of the chosen layer (1-mm) as the depth of calculated dose. This is the reason why the starting points for calculation of all doses were at 0.5-mm depth and not at 0 mm. Due to transport of the

low energy electrons, it was also important to use the PRESTA extension¹⁷.

Modeling of the beam was based on the multiple-source model¹¹. The multiple-source model is used to simulate particles coming from different parts of an accelerator as coming from different sub-sources. This approach is possible since particles from different components of a linear accelerator have different energies, angular and spatial distributions¹⁸.

The point source of monoenergetic electrons simulated the particles coming directly from the vacuum window and traversing the scattering foil and the monitor chamber. 200 nanometers of gold and 1 mm polyamide slabs were interposed in the beam to simulate scattering foil and monitor chamber. The geometrical details were available according to the manufacturer’s specifications or our own measurements. The energy of electrons at the exit vacuum window of the accelerator was adjusted to match the same R_{50} as measured data. It was done in conditions of the same opening of collimator blocks and electron applicator as during the treatment, but at SPD = 100 cm.

The electron and photon cutoffs determine the energy thresholds below, which the transport of the individual particle stops, its energy is deposited, and the particle is discarded. They were set to ECUT = 0.521 and PCUT = 0.01 MeV. The thresholds for production of the secondary particles were set to AE = 0.7 MeV for electrons and AP = 0.01 MeV for photons. Each calculation contained 10 millions cases for SPD = 100 cm, and 60 millions cases for SPD = 350 cm to obtain the estimated uncertainty in the resulting values of < 1%.

Results

The electrons scattered in the beam defining devices (collimator and electron applicator) have significantly lower mean

energy and larger mean angle between particles and the central axis than direct electrons¹⁸. Based on this, we assumed that the majority of those particles will not reach the treatment plane at the distance of 3.5 m from the source and thus can be ignored. To check this assumption we compared the measured to the calculated depth dose curves, as well as the measured and calculated dose profiles at SPD of 100 cm and 350 cm (Figures 2–5). For this purpose, the beam was collimated in the HOWFAR subroutine by simply discarding electrons and photons that passed through the jaws and electron applicators.

About 20% of electrons in the beam arise from the scattering on the collimator and the electron applicator¹¹. Since we simply discarded these soft electrons there appeared a difference between the calculated and the measured depth dose curves, but only in the 'build-up' region (Figure 2). The comparison of dose profiles shows expected discrepancy at the edges of the beam (Figure 3) caused by the simplification of the MC model.

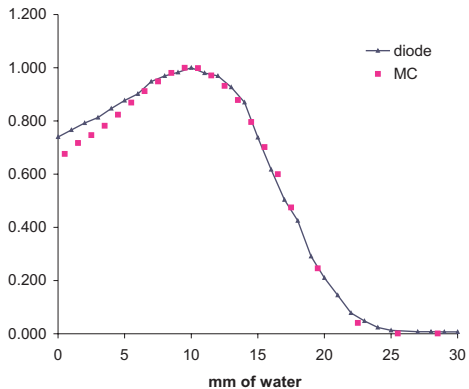


Fig. 2. Comparison of the measured and the MC calculated depth dose curves for the 25 x 25 cm² field at the 100 cm distance. The energy of the monoenergetic electron beam is adjusted in a way that R_{50} values of the measured and calculated depth dose curves match.

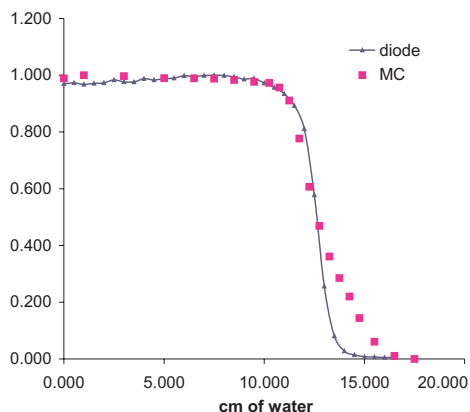


Fig. 3. Comparison of the measured and the MC calculated dose profile for the $25 \times 25 \text{ cm}^2$ field at the 100 cm distance.

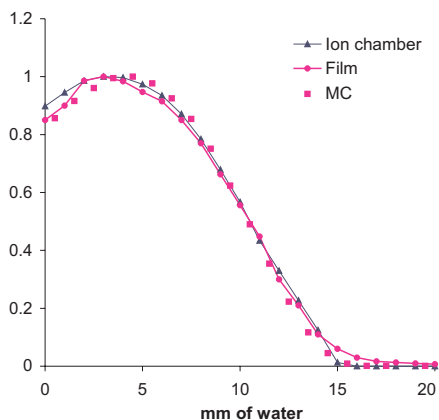


Fig. 4. Comparison of the film, ion chamber and MC results for a PTW solid phantom irradiated with one horizontal TSET beam.

The next step in testing our assumption was to compare Marcus ion chamber with the MC simulation for SPD = 350 cm. Also, we compared the obtained film measurements with ion chamber measurements. The results of film and ion chamber dosimetry in the PTW solid phantom coupled with MC calculations, for a horizontal TSET beam, are shown in Figures 4 and 5. All measurements are expressed in cm of water.

There is an improvement in the MC curves, and the difference in the 'build-up' region from ion chamber measurements is less than 5%. This confirms our assumption that the majority of the soft electrons from the beam defining system are absorbed in the additional 2.5 m layer of air and deflected out of the measuring region. The latter was caused by a larger mean angle between particles and the central axis in comparison to direct electrons¹⁸. Based on that, we simplified the multiple-source MC model of the beam and discarded all particles from the beam defining devices.

The film showed good agreement with ionization chamber measurements, except in the 'build-up' region of the depth

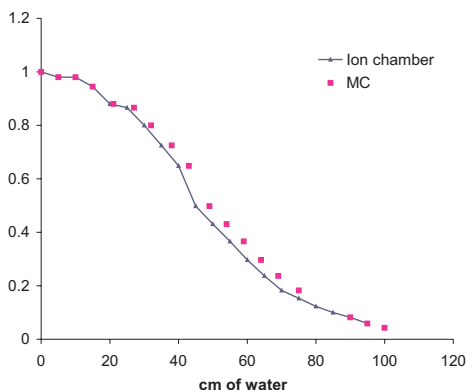


Fig. 5. Dose profiles of one horizontal TSET beam measured by the ion chamber and calculated using the MC simulation.

dose curve. This artifact, indicating a lower depth dose near the surface, was shown before⁸. The artifact may be attributed to the possible misalignment of the film edge with the surface of the phantom or the presence of thin layers of air on both faces of the film¹⁴. To minimize the artifact we exposed the bear film (without envelope) and as accurately as possible we aligned the film into the phantom slabs

that were tightly pressed together using a screw and a nut. Still, a part of this discrepancy can be attributed to the increased scatter associated with the high atomic number of the emulsion¹⁴. Since the MC modeling results were adequate for 'in-air' measurements, we compared calculations and measurements in treatment conditions using cylindrical phantom. For measurements in a cylindrical phantom we used film dosimetry. To test the model and show possible variations of a depth dose curve we measured two different orientations of the cylindrical phantom. The first cylinder is normally oriented to the beam axis and rotated around the axis of the phantom (Figure 6a). This orientation represents positions of a trunk during the TSET. The axis of the second cylinder is parallel to the beam axis and the phantom is then rotated around the

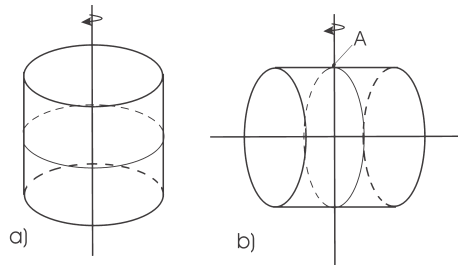


Fig. 6. Experimental arrangement of cylindrical phantoms for measuring electron depth dose curves in multiple fields' conditions. The phantom represents a) the trunk and b) the shoulders during the TSET.

axis normal to the phantom's axis (Figure 6b). This orientation of the cylindrical phantom represents positions of shoulders during the TSET.



Fig. 7. The photograph of a film exposed to the six pairs of TSET beams in a cylindrical phantom rotated around the phantom axis. This cylindrical phantom represents the trunk of an average patient during the treatment. This is the measurement of the depth dose curve that is predicted for all the points of the body during the TSET⁹. The hole in the middle of the film is made for a screw used for pressing the phantom slabs more tightly.

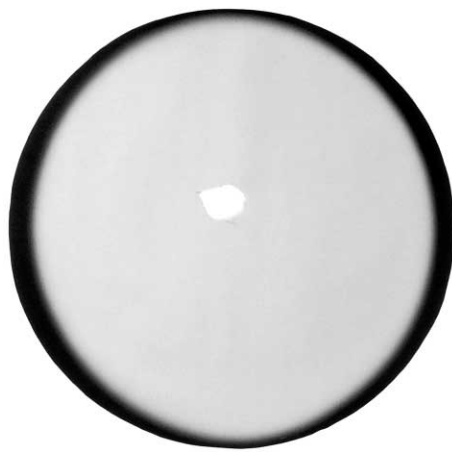


Fig. 8. The photograph of a film exposed to the six pairs of TSET beams in a cylindrical phantom rotated around the axis normal to the phantom's axis. The measurement represents the rotation of the patient's shoulder during the TSET. The hole in the middle of the film is made for a screw that is used for pressing the phantom slabs more tightly.

We chose those two orientations of body cylinders because those were the simplest for experimental arrangement. In the first orientation the angle of incident electrons is closest to 90 degrees, so the penetration of the beam is the largest. In second orientation incident electrons are tangential to the point A on the cylinder and the penetration of the beam in that point is the shallowest.

The Figures 7 and 8 show the film measurements for those orientations of the cylindrical phantom.

The Figures 7 and 8 show expected differences in shape of dose distributions when varying the longitudinal orientation of body cylinders.

The depth dose curves were calculated both ways (film densitometry and MC). In the film shown in the Figure 8 we calculated the depth dose curve for the point on the top of the film (point A in the Figure 6b) because it differs the most from the usually predicted by measurements given in Figure 7.

The densitometry of the film, shown in the Figure 7, was taken along a film radius coincident with a beam axis and a film radius midway between two such radii. We got two matching curves only differing in 7% at the surface of the phantom. This made possible the approximation that the dose at specified depth is equal all around the phantom. Since in the AUSGAB subroutine of the DOSRZ code the dose is scored between the specified planes and radii (in the whole cylindrical regions), we calculated the depth dose curve as if only one pair of the beams was employed.

When the cylindrical phantom is rotated as in the Figure 6b, depth dose curves along film radii are different for each point around the phantom. This is the reason that we made a small change in the AUSGAB subroutine. We modified it to score the dose only in the areas of interest and not in the whole cylinders. In the Figure 8, the chosen area was 1 cm

wide along the radius normal to the beam axis (in the Figure 6b it is the radius that contains the point A). The dose was calculated for all the six dual fields, changing the angle of the beam in respect to the cylinder axis.

As can be seen from the Figure 9, all calculated depth dose curves agree with the film measurements within 1–2 mm or 5 % of the maximum dose, except in the 'build-up' region. In the 'build-up' region the film underestimates dose, as shown in comparison to the ion chamber measurements (Figure 4).

The Figure 9 also shows a significant difference between the calculated depth dose curves (a) and (b) because of different orientations of cylindrical phantom.

A measurement of other orientations of the cylindrical phantom was almost impossible due to difficulties in setting up the phantom.

We calculated depth dose curves for a number of orientations of the cylinder by simply changing the angle of the beam in respect to the phantom. Since the angle of the beam was always less than 90 degrees in respect to the cylinder, doses at depths in the chosen points of the simu-

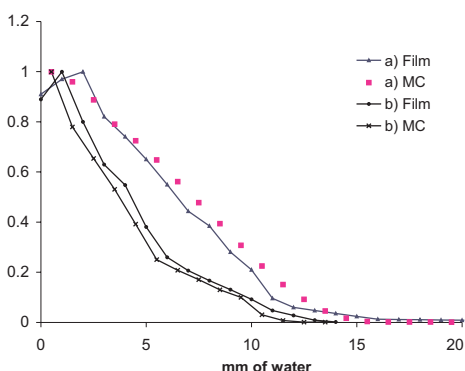


Fig. 9. Comparison of the film-measured and MC-calculated depth dose curves in the points on the top of the films of (a) Figure 7 and (b) Figure 8 for 1 cm wide area along the film radius that contain point A showed on Figure 6b.

lated cylinders were always less than usually predicted by the measurements shown in the Figure 7.

Discussion

We use the Monte Carlo modeling to simulate the TSET, with the 'six-dual-field' technique. The multiple-source MC model of the beam is done assuming that the majority of the particles from beam defining devices are absorbed in the additional 2.5 m of air layer (because of their lower energy and wider angular distribution). The validity of the assumption was backed up by comparing calculations with measurements for standard (SPD = 100 cm) and treatment (SPD = 350 cm) conditions. We also compared the film measurements and the MC calculations in the cylindrical phantom. The comparison of results showed good match. The difference of about 5 percent is found in the 'build-up' region when the model is compared to the film measurements. We compared the film measurements with the ion chamber measurements and found that the film underestimates the dose near surface. That artifact was reported and explained previously^{8,14}.

The MC model can be useful during the implementation of the TSET to avoid a large number of measurements that has to be done while adjusting the depth dose curve to match curve required by clinicians. Adjusting is done by measuring dose distributions for different combinations of electron energies, thickness of the electron scatterer and distances between the scatterer and the treatment plane¹⁰. Except for the calculations of depth dose curves for one horizontal beam (needed for energy representation) the model can be used for beam profiles calculations needed for combining beams to cover large areas. Therefore, lots of 'in-air' measurements can be avoided when assess-

ing the appropriate depth dose curve and uniformity over a treatment plane.

Usually, dose data for multiple field situations^{6,8,10} are measured in a cylindrical phantom. During the TSET, the depth dose curves in any point of a patient's body are predicted to be the same as measured in a phantom of 30 cm in diameter, normally oriented to the beam axis^{10,12}. This cylinder represents the trunk of an average patient. The film measurement of one possible different orientation of the cylindrical phantom is shown in the Figure 8 and represents positions of shoulders during the TSET. From this figure it can be concluded that doses at depths can be significantly different from the predicted ones. This is valid in the case of different diameters⁸, and also in different orientations of body cylinders (curves (a) and (b) in the Figure 9). We chose those two orientations of cylindrical phantom because they are the simplest for the experimental arrangement. In the first orientation of the cylinder (Figure 6a) the penetration of the beam is the largest and when the cylinder is oriented as in the Figure 6b the penetration of the beam in the point A is the shallowest because of the angles between the beams and the cylinders. We also modeled orientations of the cylinder between those two orientations and, as expected, the depth dose curves were between the two measured. Since measurements are almost impossible in variety of diameters and positions of body cylinders, one way of predicting doses along the patient's skin can be the MC model of the TSET beams.

In general, the TSET is not a routine technique; therefore the extended time needed for simulations may not be a disadvantage.

Acknowledgement

This work was supported by the Croatian Ministry of Science and Technology grant.

REFERENCES

1. JONES, G. W., R. T. HOPPE, E. GLATSTEIN, Hemat. Oncol., 9 (1995) 1057. — 2. MORDACCHINI, C., P. ANTOGNONI, L. CONTE, Radiol. Med., 80 (1990) 143. — 3. JONES, G. W., R. WONG, J. KASTIKAINEN, N. FARRAR, L. R. FOX-GOGUEN, Sur. Int. J. Radiat. Oncol. Biol. Phys., 57 (2003) 291. — 4. SMITH, B. D., L. D. WILSON, Oncology (Huntingt.), 17 (2003) 1419. — 5. MARGARETIĆ, D., D. FAJ, I. TOMAŠ, B. DMITROVIĆ, Z. KRAJINA, Croat. Med. J., 43 (2002) 342. — 6. FAJ, D., Z. KRAJINA, M. BISTROVIĆ, D. GUGIĆ, D. MARGARETIĆ, N. BELAJ, Libri Oncol., 29 (2001) 17. — 7. EDELSTEIN, G. R., T. CLARK, J. G. HOLT, Radiology, 108 (1978) 691. — 8. NIROOMAND-RAD, A., M. T. GILLIN, R. KOMAKI, R. W. KLINE, D. F. GRIMM, Int. J. Rad. Biol. Phys., 12 (1986) 415. — 9. PAGE, V., A. GARDNER, C. J. KARZMARK, Radiology, 94 (1970) 635. — 10. AAPM, Report No 23. (American Institute of Physics, New York, 1988). — 11. MA, C. M., B. A. FADDEGON, D. W. O. ROGERS, T. R. MACKIE, Med. Phys., 24 (1997) 401. — 12. FRAAS, B. A., P. L. ROBERSON, E. GLATSTEIN, Radiology 146 (1983) 811. — 13. TWAITES, D. I., Phys. Med. Biol. 30 (1985) 41. — 14. ICRU: Report 35. (ICRU, Bethesda, 1984). — 15. AAPM TG-21, Med. Phys., 10 (1983) 741. — 16. NELSON, W. R., H. HIRAYAMA, D. W. O. ROGERS: SLAC-Report-265. (Stanford Linear Accelerator Center, Stanford, 1985). — 17. BIELAJEW, A. F., D. W. O. ROGERS, Nuclear Instrum. Methods, 18 (1987) 165. — 18. KAPUR, A., C. M. MA, E. C. MOK, D. O. FINDLEY, A. L. BOYER, Phys. Med. Biol., 43 (1998) 3479.

D. Faj

Department of Oncology and Radiotherapy, University Hospital »Osijek«, J. Huttlera 4, 31000 Osijek, Croatia

MODEL LIJEČENJA KORIŠTENJEM »SIX-DUAL-FIELD« TEHNIKE ZRAČENJA CIJELE KOŽE

S A Ž E T A K

Prilikom uvođenja »six-dual-field« tehnike zračenja cijele kože na radioterapijski odjel potrebno je učiniti veliki broj mjerenja. Potrebna raspodjela doze u dubini, te jednoličnost doze u terapijskoj ravnini postiže se kombinacijom određenih parametara zračenja. Za svaku kombinaciju vrši se niz mjerenja. Da bi smanjili broj potrebnih mjerenja modelirali smo zračenje Monte Carlo simulacijom elektronskog transporta, te ga usporedili s mjerenjima. Računate vrijednosti u terapijskoj ravnini razlikuju se od mjerenih za manje od 5%. Model smo iskoristili i za procjenu promjene doze u ovisnosti o zakrivljenosti i promjeni položaja tijela bolesnika. Bolesnika smo aproksimirali u niz cilindara različitih promjera i orijentacija. Usporedili smo mjerenja i računicu za dvije orijentacije cilindričnih fantoma koje je najjednostavnije postaviti za mjerenja. Usporedba je pokazala točnost modela, te smo model iskoristili za izračun doza u različito orijentiranim cilindričnim fantomima.